

A Hessian-Based Field Deformer for Real-Time Topology-Aware Shape Editing

YUNXIAO ZHANG, Shandong University, China

ZIXIONG WANG, Shandong University, China

ZIHAN ZHAO, Shandong University, China

RUI XU, Shandong University, China

SHUANGMIN CHEN*, Qingdao University of Science and Technology, China

SHIQING XIN, Shandong University, China

WENPING WANG, Texas A&M University, USA

CHANGHE TU, Shandong University, China



Fig. 1. We present 17 groups of editing results produced by volunteers. Our interactive system operates at 30 FPS, and supports both topology editing and geometry editing.

Shape manipulation is a central research topic in computer graphics. Topology editing, such as breaking apart connections, joining disconnected ends, and filling/opening a topological hole, is generally more challenging than geometry editing. In this paper, we observe that the saddle points of the signed distance function (SDF) provide useful hints for altering surface topology deliberately. Based on this key observation, we parameterize the SDF into a cubic trivariate tensor-product B-spline function F whose saddle points $\{s_i\}$ can be quickly exhausted based on a subdivision-based root-finding technique coupled with Newton's method. Users can select one of the candidate points, say s_i , to edit the topology in real time. In implementation, we add a compactly supported B-spline function rooted at s_i , which we call a *deformer* in this paper, to F , with its local coordinate system aligning with the three eigenvectors of the Hessian. Combined with ray marching technique, our interactive system operates at 30 FPS. Additionally, our system empowers users to create desired bulges or concavities on the surface. An extensive

user study indicates that our system is user-friendly and intuitive to operate. We demonstrate the effectiveness and usefulness of our system in a range of applications, including fixing surface reconstruction errors, artistic work design, 3D medical imaging and simulation, and antiquity restoration. Please refer to the attached video for a demonstration.

CCS Concepts: • **Computing methodologies** → **Mesh geometry models**.

Additional Key Words and Phrases: signed distance function, cubic B-spline, topology editing, Morse theory, saddle point, Hessian matrix

ACM Reference Format:

Yunxiao Zhang, Zixiong Wang, Zihan Zhao, Rui Xu, Shuangmin Chen, Shiqing Xin, Wenping Wang, and Changhe Tu. 2023. A Hessian-Based Field Deformer for Real-Time Topology-Aware Shape Editing. In *SIGGRAPH Asia 2023 Conference Papers (SA Conference Papers '23)*, December 12–15, 2023, Sydney, NSW, Australia. ACM, New York, NY, USA, 10 pages. <https://doi.org/10.1145/3610548.3618191>

*Corresponding author

Permission to make digital or hard copies of all or part of this work for personal or classroom use is granted without fee provided that copies are not made or distributed for profit or commercial advantage and that copies bear this notice and the full citation on the first page. Copyrights for components of this work owned by others than the author(s) must be honored. Abstracting with credit is permitted. To copy otherwise, or republish, to post on servers or to redistribute to lists, requires prior specific permission and/or a fee. Request permissions from permissions@acm.org.

SA Conference Papers '23, December 12–15, 2023, Sydney, NSW, Australia

© 2023 Copyright held by the owner/author(s). Publication rights licensed to ACM.

ACM ISBN 979-8-4007-0315-7/23/12...\$15.00

<https://doi.org/10.1145/3610548.3618191>

1 INTRODUCTION

Shape manipulation is an active area of research in geometric modeling due to its ever-widening range of applications in editing tools for industrial and artistic design, such as computer-aided design [Ito et al. 2021; Xiong and Zimin 2022], digital sculpting [Mandal et al. 2022; Moo-Young et al. 2021], and character design [Hu and Wen 2019; lin Yu and Tsao 2022]. This topic is challenging since complex mathematical formulations have to be hidden behind an intuitive

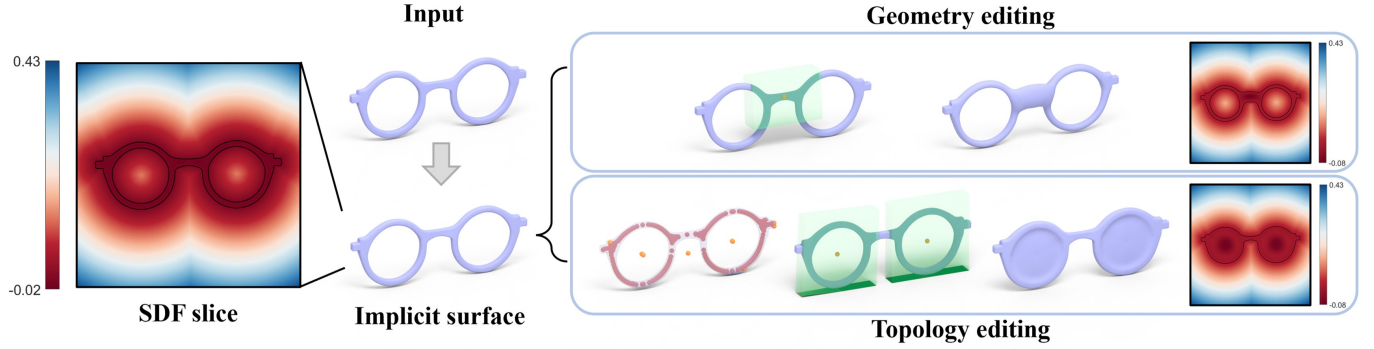


Fig. 2. A typical workflow of shape manipulation with our interactive system involves operating on the implicit representation F that approximates the real signed distance function. For a base point (in orange) on the surface, among the three eigenvectors of the Hessian of F , two align with the principal curvature directions and one aligns with the normal direction. This mathematical fact enables us to define a geometry editing deformer (in green) using the local coordinate system spanned by the three eigenvectors (see the top row). Furthermore, we observe that the saddle points of F are useful for determining deliberate alterations in the surface topology. Based on this observation, one can easily edit the topology by breaking apart connections, joining disconnected ends, and filling or opening a topological hole (see the bottom row).

user interface with which the behavior of shape manipulation can be implemented in a sufficiently efficient and robust manner.

Shape manipulation can generally be divided into two categories: topology editing and geometry editing. Topology editing allows users to modify the surface topology by breaking apart connections, joining disconnected ends, and filling or opening topological holes. Geometry editing, on the other hand, aims to manipulate surface variations. Topology editing is more challenging as it involves topological changes and is not easily performed on a triangle mesh. Some research has been done on updating implicit representations based on user-specified input strokes [Angles et al. 2017; Ju et al. 2007], but the interaction system is difficult to operate.

In this paper, we examine the topology editing challenge through the lens of two distinct perspectives. Firstly, implicit representations such as the signed distance function (SDF) are expressive in topology control but not intuitive for users to operate. To overcome this challenge, we parameterize the SDF into a cubic trivariate tensor-product B-spline function, which can be formulated into solving a sparse linear system. Secondly, if s is a saddle point of the SDF, then one can easily change the surface topology around s by adding a deformer rooted at s to the SDF until the sign of the function value at s alters. To be more specific, 1-saddle points, where the Hessian matrix of the SDF has only one negative eigenvalue, reveal unstable topology where one can break apart an existing connection or join two disconnected ends. Instead, 2-saddle points reveal unstable topology where it is easy to fill or open a topological hole. Our research is motivated by these two aspects.

In implementation, we first fit the given mesh surface into a cubic trivariate tensor-product B-spline function F , whose saddle points can be quickly exhausted by examining every cubic element. The saddle points enable users to select the preferred one, say s_i , and edit the corresponding part. The computational task involves adding to F a compactly supported B-spline function rooted at s_i , with its local coordinate system aligning with the three eigenvectors of the Hessian. Combined with ray marching technique [Hart 1996], our interactive system operates at 30 FPS even on an entry-level graphics processing unit.

Our contributions are three-fold:

- (1) We present a novel topology editing method based on the observation that the saddle points of the signed distance function (SDF) offer useful hints for determining deliberate alterations in surface topology.
- (2) We parameterize the SDF into a cubic trivariate tensor-product B-spline function, allowing for quick identification of saddle points.
- (3) We developed a real-time interactive system that combines topology editing with geometry editing. The system runs at over 30 FPS, leveraging ray marching technique for rendering [Hart 1996]. An extensive user study indicates that our system is user-friendly and intuitive to operate.

2 RELATED WORK

A significant amount of research has been conducted on shape manipulation in recent decades. In this section, we review the relevant literature and categorize it based on specific representation forms.

Parametric/Polygonal methods. Most existing methods manipulate shape on triangle meshes or parametric surfaces by predicting displacement for influenced mesh vertices or parametric subdomains. Fowler [1992] and Wong et al. [2000] proposed a method for direct manipulation of the surface using a B-spline tensor product representation. Terzopoulos and Qin [1994] developed a dynamic generalization of the NURBS model for physically intuitive surface manipulation. Peng et al. [2018] advocated predicting users' editing behavior to enable automatic editing. Despite their success in geometry editing, these surface representations are weak in topology editing because they focus on the surface itself, regardless of its embedding in three-dimensional space. Some methods [Fu et al. 2004] consider topology requirements but involve time-consuming proximity query operations.

Volume-based methods. Galyean and Hughes [1991] first introduced volumetric representation to interactive modeling in 1991, and proposed a sculpting method based on grid-based tessellations (voxmap). Perry and Frisken [2001] proposed a 3D sculpting method

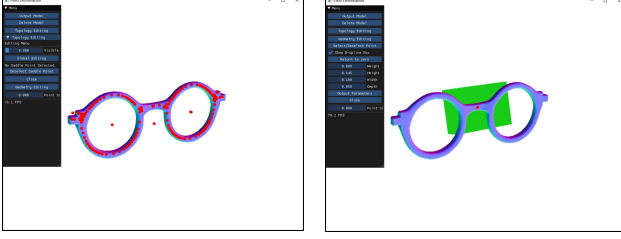


Fig. 3. The interface of our interactive system. In the left figure, we show the saddle points (in red) of the SDF. In the right figure, we designate a base point where we intend to edit the geometry. The green box illustrates the area of influence, facilitating user adjustments.

based on Adaptively Sampled Distance Fields (ASDF), but the approach suffers from low interaction speed. Benefiting from the technique for storing regular virtual grids [Barthe et al. 2002; Ferley et al. 2000, 2001], Bærentzen [1998] used an octree to assist volume sculpting, resulting in higher interaction speed and less memory usage. Schmidt et al. [2005] utilized hierarchical implicit volume models (blob-trees) as the underlying shape representation for interactive modeling in 2005. Later, some sketch-based modeling techniques [Ju et al. 2007] are proposed to facilitate editing the topology of 3D models. The primary drawback of the aforementioned volume-based methods is that editing the volume lacks the intuitiveness of editing the surface.

Continuous implicit function-based methods. Implicit functions offer a flexible representation, enabling the definition of complex and smooth models with arbitrary topology. Hart [1998] introduced the relationship between the topology of implicit surfaces and critical points. Building upon this relationship, Stander and Hart [1997] devised a polygonization algorithm that guarantees topology, based on the observation that changes in the sign of the function value at critical points lead to changes in topology, provided that the analytic form of the implicit function is given. However, their methodology is specifically designed to extract the zero level-set polygonal surface from a given implicit function with an analytic form, rather than use of critical points for controlling the implicit surface topology and the related modeling tools. Sharf et al. [2007] and Yin et al. [2014] proposed to use implicit representations to drive the topology change of point clouds. Canezin et al. [2016] proposed a topology-aware reconstruction method. But the run-time performance is insufficient for supporting real-time user interaction. Museth et al. [2002, 2005] and Eyiurekli and Breen [2010] introduced a set of free-form editing operators based on level-set volume representations of scalar fields. However, these methods require solving partial differential equations during each edit, and thus cannot satisfy interaction requirements. Pasko et al. [2005] and Bernhardt et al. [2010] provided a set of blending operators that combine two scalar functions, but this is not intuitive for users to explicitly control topology. Gourmel et al. [2013] and Angles et al. [2017] used gradient-based operators to manipulate shapes, but their approach cannot be used for general shapes. In summary, continuous implicit representations are flexible in accommodating changes in geometry and topology. However, the key challenge lies in quickly identifying the intended area for

topology editing and updating the implicit representation in a manner that is easy to operate and immediately visualizes changes in topology and geometry.

3 HESSIAN-BASED FIELD DEFORMER

We assume that the standard input is a polygonal mesh surface. However, it's important to note that our algorithm is also compatible with other forms of surface representation. The workflow of our framework is outlined in Fig. 2, while Fig. 3 displays the interface of our interactive system. The workflow consists of three distinct steps: 1) trivariate B-spline generation, 2) exhaustive search of saddle points, and 3) topology editing using a Hessian based deformer. To ensure real-time interaction, we utilize the ray marching technique [Hart 1996] to render the 3D objects. We will elaborate on each step in the following subsections.

3.1 Trivariate B-Spline Generation

Without loss of generality, we normalize the input model into $[0, 1]^3$. At the same time, we partition the unit space into regularly structured grid cells, where each grid vertex is denoted by \mathbf{g}_{ijk} . Let w be the distance between two adjacent grid vertices, and N be the number of grid cells along each dimension, i.e., $N = 1/w$. All the grid vertices define a set

$$G = \{\mathbf{g}_{ijk} : i, j, k = 0, 1, \dots, N\}. \quad (1)$$

The signed distance function (SDF), a commonly used implicit representation, can be readily derived from other representations, such as the point cloud [Huang et al. 2019] and polygonal mesh [Jacobson et al. 2013]. Furthermore, it has the capability to present the topological information of any level-set in space.

Tensor-product B-splines [Rouhani et al. 2014; Tang and Feng 2018] have been extensively utilized to approximate the SDF. Owing to the local-support and non-oscillation [Hall and Meyer 1976] properties of the basis functions, we employ a cubic trivariate tensor-product B-spline function in this paper to parameterize the SDF, thereby enabling local topology editing. The normalized cubic trivariate tensor-product B-spline basis rooted at the grid point \mathbf{g}_{ijk} can be written as

$$B_{ijk}(\mathbf{q}) = B\left(\frac{\mathbf{q} - \mathbf{g}_{ijk}}{w}\right). \quad (2)$$

$$B(\mathbf{q}) = b(x)b(y)b(z), \quad \text{with } \mathbf{q} = (x, y, z), \quad (3)$$

where $b(t)$ is the univariate cubic B-spline basis, i.e.,

$$b(t) = \begin{cases} -\frac{1}{6}t^3 + t^2 - 2t + \frac{4}{3} & t \in [1, 2] \\ \frac{1}{2}t^3 - t^2 + \frac{2}{3} & t \in [0, 1] \\ -\frac{1}{2}t^3 - t^2 + \frac{2}{3} & t \in [-1, 0] \\ \frac{1}{6}t^3 + t^2 + 2t + \frac{4}{3} & t \in [-2, -1] \\ 0 & \text{otherwise.} \end{cases} \quad (4)$$

To this end, we intend to represent the SDF in the following form

$$F(\mathbf{q}) = \sum_{i,j,k} \alpha_{ijk} B_{ijk}(\mathbf{q}), \quad (5)$$

where α_{ijk} is the unknown coefficient to be determined.

By taking the polygonal mesh as the input, we query the SDF values for any grid point in G using the signed distance query

Table 1. Categorization of critical points via Hessian analysis

Critical point	Sign		
	λ_1	λ_2	λ_3
Minimum point	+	+	+
1-saddle point	-	+	+
2-saddle point	-	-	+
Maximum point	-	-	-

routine in libigl [Jacobson et al. 2018], and produce the following linear system:

$$A\alpha = c, \quad \text{with} \quad \alpha = \{\alpha_{ijk}\}, \quad (6)$$

where c is given by the SDF values at grid vertices, and each entry of A is computed as

$$B_{ijk}(\mathbf{g}_{i'j'k'}), \quad (7)$$

where i, j, k traverse each basis function while i', j', k' traverse each grid point. It is evident that A is a symmetric and sparse matrix. Furthermore, $\{B_{ijk}\}$ defines a group of basis functions that are linearly independent of each other, from which the invertibility of A can be easily verified. Therefore, the coefficients α can be found immediately by simply calling the Conjugate Gradient Method [Hestenes et al. 1952]. To this end, we accomplish interpolating the SDF using a cubic trivariate tensor-product B-spline function that enables us to analyze the first-order and second-order properties of the SDF.

3.2 Exhaustive Search of Saddle Points

Saddle points. \mathbf{q} is said to be a critical point of F if the gradient $\nabla F|_{\mathbf{q}}$ vanishes. As shown in Tab. 1, the critical points of F can be further divided into maximum points, minimum points, 1-saddle points, and 2-saddle points, depending on how many negative eigenvalues the Hessian of F owns.

Interestingly, a strong correlation exists between the saddle points of the SDF and the instability of the surface topology, as indicated in [Stander and Hart 1997]. Specifically, 1-saddle points expose unstable topology where existing connections can be severed or disconnected ends can be joined. Conversely, 2-saddle points expose unstable topology where topological holes can be easily filled or opened. Figure 4 illustrate examples of 1-saddle, 2-saddle, maximum and minimum points, respectively.

Exhaustive search. To exhaustively search the saddle points of F , it is necessary to identify saddle points within each grid cell. This can be accomplished using the subdivision-based root-finding technique [Mourrain and Pavone 2009] to subdivide a grid cell into eight subcells. In our implementation, we establish a maximum subdivision level of 1 to prevent the generation of an excessive number of saddle points (which could potentially be infinitely many). Subsequently, we use each subcell center as initialization and apply Newton’s method to refine the position of the saddle. It’s important to note that the number of iterations is capped at 20.

3.3 Field Deformer for Topology Editing

As Figure 5 shows, we precompute all the saddle points $S = \{\mathbf{s}_i\}$ that indicate unstable topological structures. In general, users can

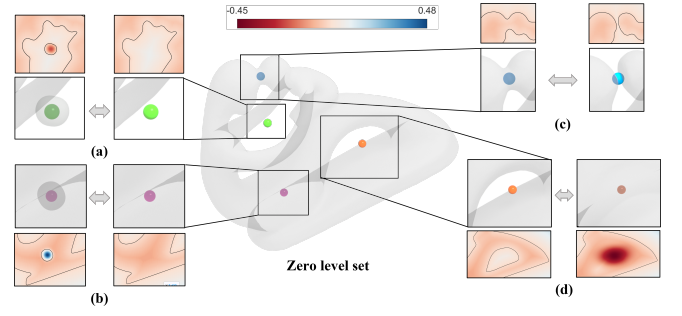


Fig. 4. The critical points of the Signed Distance Function (SDF) are closely related to topological structures and can be classified into minimum (purple), 1-saddle (blue), 2-saddle (orange), and maximum (green) based on the Hessian of the SDF. (a-b) Maximum and minimum points reflect stable topological structures. When users make local changes to the SDF, it may produce an outlier surface that cannot be connected to the base surface. To prevent this, our system does not allow users to select maximum and minimum points for editing. (c) 1-saddle points correspond to local adhesion and separation around a thin handle. (d) 2-saddle points correspond to a tunnel area where a topological hole can be filled or opened.

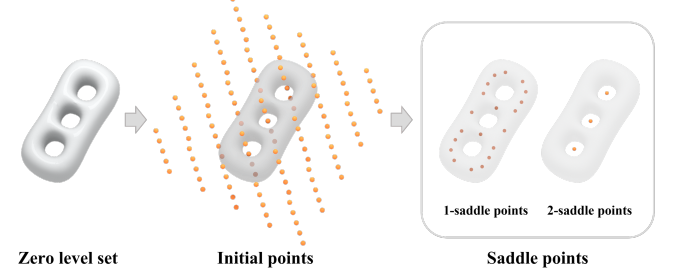


Fig. 5. The process of exhaustively searching for saddle points.

select one of them, say \mathbf{s}_i , and express their intention of topology editing. The typical way for editing the implicit function F is as follows:

$$F_{\text{new}}(\mathbf{q}) = F(\mathbf{q}) + \sum_{\mathbf{s}_i \in S} D_{\mathbf{s}_i}(\mathbf{q}), \quad (8)$$

where $D_{\mathbf{s}_i}(\mathbf{q})$ serves as the deformer rooted at \mathbf{s}_i .

We suppose that the Hessian can be decomposed into

$$H = Q\Lambda Q^T, \quad (9)$$

where Λ is a diagonal matrix keeping the three eigenvalues while Q encodes the three eigenvectors. For local shape manipulation, we need to align the deformer $D_{\mathbf{s}_i}(\mathbf{q})$ with the three eigenvectors of H :

$$D_{\mathbf{s}_i}(\mathbf{q}) = \beta_{\mathbf{s}_i} B \left(W_{\mathbf{s}_i}^{-1} Q^T (\mathbf{q} - \mathbf{s}_i) \right), \quad (10)$$

where $W_{\mathbf{s}_i}$ represents a diagonal matrix that defines the scaling factors along three distinct directions and $\beta_{\mathbf{s}_i}$ is used to tune the influence of the deformer at \mathbf{s}_i .

Let the saddle \mathbf{s}_i be projected onto \mathbf{s}'_i , a point lying on the current surface. Among these eigenvectors, we take the eigenvector that closely aligns with the vector $\mathbf{s}_i \mathbf{s}'_i$ as the first one. Suppose that the corresponding eigenvalue is λ_1 . For the two remaining eigenvalues, we select one of them that has the opposite sign to λ_1 , and label the corresponding eigenvector as the second one. If both the two

remaining eigenvalues own the opposite sign, we prioritize the one with a larger absolute value. To this end, the weighting parameters for the first and second eigenvectors are as follows:

$$W_{s_i}^{(1)} = 2 |F(s_i)|, W_{s_i}^{(2)} = 4w,$$

where w is the gap between two adjacent grid points. Finally, $W_{s_i}^{(3)}$ is set in reference to $W_{s_i}^{(1)}$ if their corresponding eigenvalues are of the same sign. Otherwise, $W_{s_i}^{(3)}$ is set in reference to $W_{s_i}^{(2)}$. In other words, the weight ratio equals the ratio of the values of their corresponding eigenvalues.

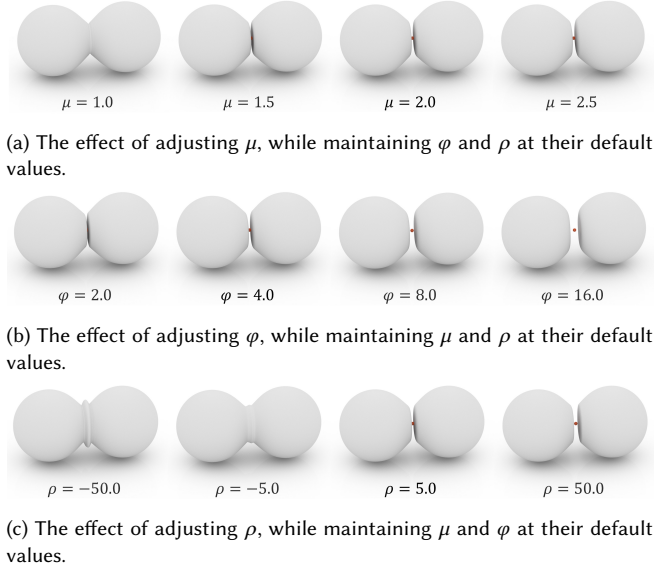


Fig. 6. By individually adjusting the weighting parameters, one can observe distinct effects. We denote $W_{s_i}^{(1)} = \mu |F(s_i)|$ and $W_{s_i}^{(2)} = \varphi w$. The default values of μ and φ are 2 and 4 respectively. Additionally, $\rho = -\frac{\beta_{s_i}}{F(s_i)}$ is used to define the overall weight of the s_i -based deformer and set to 5 by default.

Under the default weight setting, the overall implicit function can be written as

$$F_{\text{new}}(\mathbf{q}) = \sum_{i,j,k} \alpha_{ijk} B_{ijk}(\mathbf{q}) + \sum_{s_i \in S} \beta_{s_i} B \left(W_{s_i}^{-1} Q^T(\mathbf{q} - \mathbf{s}_i) \right). \quad (11)$$

To this end, users can select their preferred saddle point s_i and subsequently modify the influence β_{s_i} to generate a new implicit function, the zero level-set surface of which defines the new surface. For example, if one increases β_{s_i} from negative to zero, $F_{\text{new}}(s_i)$ approaches 0, making the surface locally deformed toward the point s_i . It can be imagined that when one continues to increase β_{s_i} such that $F_{\text{new}}(s_i)$ becomes positive, the topology will undergo a sudden change, i.e.,

$$F_{\text{new}}(s_i) = \sum_{i,j,k} \alpha_{ijk} B_{ijk}(s_i) + \beta_{s_i} B(0) \geq 0, \quad (12)$$

where $B(0)$ is $8/27$. The above inequality implies that a topological flip between adhesion and separation may occur if

$$\beta_{s_i} \geq -\frac{\sum_{i,j,k} \alpha_{ijk} B_{ijk}(s_i)}{B(0)}.$$

So we set $\beta_{s_i} = -\rho F(s_i)$, where ρ is a parameter. See Figure 6 for distinct effects of adjusting the weighting parameters.

3.4 Implementation Details

Geometry editing. In the context of topology editing, the base points for user selection are restricted to the saddle points of F . However, our approach also enables geometry editing by treating surface points as base points. Typically, the most common geometry editing scenario involves creating a bulge or concavity. For such a purpose, we utilize a similar strategy as in Section 3.3 to set the default weights for geometric editing. The only difference lies in that both $W_{s_i}^{(2)}$ and $W_{s_i}^{(3)}$ vary in reference to $W_{s_i}^{(1)}$ such that the ratios between the eigenvalues are maintained. See Figure 7

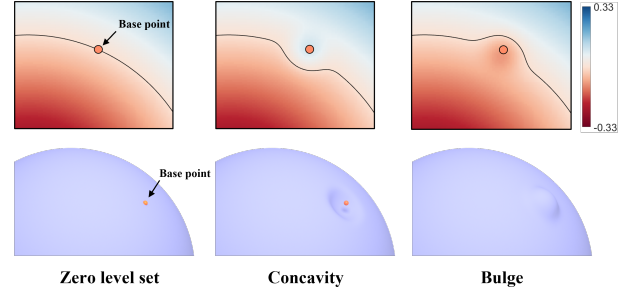


Fig. 7. Two typical situations of geometry editing based on a base point (orange).

for an example of geometry editing. Let \mathbf{p} represent a point on the surface. From differential geometry, it is known that the Hessian matrix at a surface point \mathbf{p} must have a zero eigenvalue, with the corresponding eigenvector defining the normal vector. Given that F serves as an approximate counterpart of the real SDF, we can identify the eigenvalue with the smallest absolute value and use its corresponding eigenvector as the normal vector. The other two eigenvectors naturally align with the principal curvature directions. Our Hessian-based deformer, equipped with a carefully selected set of parameters, is capable of preserving the existing anisotropic shape variation to the greatest extent possible. The anisotropic feature will be diminished if the eigenvector directions are replaced by a normal direction and two random orthogonal directions, which is referred to as a normal-based deformer in this paper. We provide a comparison between the Hessian-based deformer and the normal-based deformer in Figure 8. The comparison suggests that our Hessian-based deformer offers a more intuitive manipulation experience compared to the normal-based deformer.

High frame rate. During the process of geometry/topology editing, users may need to adjust certain parameters to visualize the deformation outcome in real time. Clearly, marching cubes are not an ideal choice as they require visiting a large number of small cubic elements. To ensure a seamless interaction experience, we

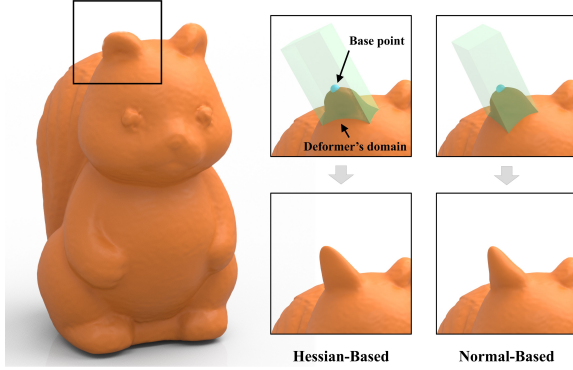


Fig. 8. Our Hessian-based deformer offers a more intuitive manipulation experience compared to the normal-based deformer.

utilize the ray marching technique [Hart 1996] to achieve a high frame rate. Additionally, it’s worth noting that the saddle points are computed only once, as minor topology editing operations do not eliminate or relocate a saddle point. Based on this assumption, it is only necessary to retain the deformers, without the need for re-computation of the saddle points.

4 USER STUDY

To assess the efficiency and user-friendliness of our interactive system, which employs the proposed field deformer for topology and geometry editing, we conducted comprehensive user studies. These studies were designed to thoroughly evaluate the interactive system’s performance. We select the sketch-based topology editing method (STEM) [Ju et al. 2007] as the baseline. The study comprised four stages: training, target reproduction, open-ended model creation, and feedback acquisition. All tasks were performed on a laptop equipped with an Intel Core i7-12700H Processor, 16GB of memory, and an NVIDIA GeForce RTX 3060 graphics processing unit.

4.1 Participants and User Training

We enlisted 15 volunteers, comprising 3 females and 12 males, aged between 18 and 30. The volunteers were undergraduate and graduate students with backgrounds in computer science education. Of these volunteers, eight have prior experience with model editing systems, while the remaining seven are novices.

We trained the participants by explaining the concepts of topology and geometry editing and introducing the tools, including our system and STEM [Ju et al. 2007], over a period of 5 minutes. To ensure that all participants were proficient in using the test tools, we asked them to complete several simple training tasks similar to our reproduction tasks.

4.2 Target Reproduction Tasks

To thoroughly demonstrate our system’s performance, we meticulously designed four representative tasks that focus on different types of topology editing: opening/filling a topological hole, breaking apart connections, and joining disconnected ends.

Task models construction. To ensure the suitability of the input/target models pair for the tasks, we manually created the input model of each task based on a selected target models using boolean operators in MeshLab [Cignoni et al. 2008]. The model is presented in the first column of Figure 9 (on Page 9).

Reproduction procedure. For each task, participants were provided with an input model and a reference target model. For comparison purposes, they were instructed to edit the input model to closely resemble the target model using both STEM [Ju et al. 2007] and our system. Each task had a maximum time limit of 5 minutes, and participants were asked to fill in a questionnaire. Additionally, the quality of the results was evaluated using common metrics.

Quantitative evaluation. We employ a combination of objective and subjective methods to quantitatively evaluate both the results and user experience.

Objectively, in order to evaluate the quality of the results in target reproduction tasks, we selected the following metrics: chamfer distance (scaled by 10^3 , using L_1 -norm) measures the fitting tightness between the two surfaces; F-Score (%) indicates the harmonic mean of precision and recall (completeness); normal consistency (%; abbreviated as ‘Normal C.’) reflects the degree to which the normals of the edited surface agree with the normals of the ground-truth surface; genus and connected components present topological measures over the edited models. As presented in Table 2 (on Page 10), our system outperforms STEM [Ju et al. 2007] in all metrics, showing that users achieved better-quality outcomes by our system within the same editing time. Compared to STEM [Ju et al. 2007] in which user-drawn sketches may not accurately convey the intended interaction, our system utilizes precomputed saddle points as interaction hints and offers a more straightforward and intuitive manipulation method.

Subjectively, all participants filled in the questionnaire including three scoring items: system fluency, system operability, and satisfaction with the editing results on a scale of 1 to 5. The statistical results are shown in Figure 10 (on Page 9). It shows that our system received high scores on all items, while STEM has poor operability and most participants were not satisfied with the editing results.

4.3 Open-ended Model Creation and User Feedbacks

To evaluate the creative freedom provided by our system, all participants were allowed to make topological and geometric changes. A selection of the results is presented in Figure 1. In Figure 11 and Figure 12 (both on Page 9), we present examples created through either topology editing or geometry editing, respectively. Upon the completion of all tasks, we conducted brief interviews with the participants to get their impressions of our system. The majority of users reported that the system was straightforward to learn and significantly reduced the complexity and learning curve associated with model editing. One beginner user remarked, “Compared to other commercial tools, this system simplifies the learning process for 3D creation. I can now effortlessly create the models I desire.”

4.4 Performance

We collected necessary statistics to demonstrate the efficiency of our system.

Time cost for implicitization and exhaustive search of saddles. Since our algorithm operates directly on the tensor-product function, the resolution of grid cells plays a crucial role in balancing the accuracy and run-time performance of implicitization and exhaustive search of saddles. The relationship between resolution and run-time costs is illustrated in Figure 13 (on Page 9). In our user study, we used a resolution of $N = 150$, as shown in Figure 9 (on Page 9). With this setting, the search cost is typically below 25 seconds and the time required to solve equations is reduced to less than 10 seconds.

Interactive speed. To evaluate the real-time performance of our system, we measured the Frames Per Second (FPS) for topology editing, geometry editing, and idle state over a 5-minute duration using two different graphics processing units: the NVIDIA GeForce GTX 1060 and NVIDIA GeForce RTX 3060, based on the same CPU. As shown in Figure 14 (on Page 9), our system operates at above 30 FPS on whether 1060 or 3060, providing a high frame rate and enabling real-time response to user operations.

5 APPLICATIONS

We present several example applications that benefit from the Hessian-based field deformer. In different application scenarios, users have the flexibility to selectively choose either saddle points or any point on the model surface based on their specific requirements.

Fixing surface reconstruction errors. Reconstructing a continuous surface from a given point cloud has always been a highly challenging task, particularly in cases where the point cloud exhibits poor quality, such as sparsity, noise, and other defects. Screened Poisson reconstruction (SPR) [Kazhdan and Hoppe 2013], one of the most classical reconstruction methods, also faces the challenge of introducing topological noise when reconstructing from low-quality point clouds. In fact, topological errors such as unexpected adhesion, separation, and holes may occur, greatly limiting its use in many practical applications. To our knowledge, the research community lacks an easy-to-use tool to fix these issues on reconstruction results. With the support of our Hessian-based field deformer, one can easily edit geometry variations or topological errors with minimal computational effort. In general, users can use our default parameters for quick geometry/topology editing or customize a set of new parameters for specific application scenarios. Figure 15 (on Page 10) illustrates several outcomes achieved by utilizing our tool to fix issues caused by SPR. It is evident that our deformer can easily recover the original topological structure without altering topologically faithful areas.

Artistic design. Designing a work of art is often a complex and intricate task. During the design process, artists need to continuously modify the topology and geometry of the model to achieve artistic and aesthetic appeal. However, existing design tools such as ZBrush, Blender, etc., struggle with direct topological modifications, which greatly hinders the design of art pieces. Our Hessian-based field deformer, on the other hand, has the ability to directly change the

topology of the model based on saddle points in an intuitive manner, providing artists with tremendous convenience. During the actual editing process, artists can select the saddle points corresponding to the area of interest to flip the local topology toward the desired structure. Refer to Figure 16 (on Page 10) for an illustration of the results achieved using our deformer.

3D medical imaging/simulation. Our method also finds application in medical imaging and simulation, allowing for the manipulation of the topology of anatomical models. This enables customized surgical planning, simulation, and educational purposes, enhancing patient-specific treatment strategies and surgical outcomes. By utilizing the Hessian-based field deformer, surgeons and researchers can interactively edit the topology of anatomical models, visualize anatomical structures, identify surgical risks, and optimize surgical strategies. For example, due to the unique topological structure of vascular tumors within the vascular system, our interactive system can rapidly and accurately locate potential vascular tumors and simulate their removal, as depicted in Figure 17 (on Page 10).

Antiquity restoration. Another application of our method involves cultural heritage restoration, specifically in the domain of antiquity conservation. These antiquities possess significant historical and cultural value. In the event of irreversible damage, physical restoration can be laborious and protracted, potentially compromising their intrinsic value. Instead, our system offers a convenient tool to identify structural issues and edit the geometry/topology within the virtual world. Figure 18 (on Page 10) showcases an example of ancient antiquity restoration by utilizing using our system. It can be seen that our system enables professionals to achieve their intentional modifications in an intuitive manner. To sum up, our interactive system can help professionals enhance their efficiency and improve restoration outcomes.

6 CONCLUSIONS

We present a Hessian-based field deformer that facilitates real-time topology-aware shape editing, guided by two primary considerations. First, a strong correlation exists between the saddle points of the SDF and the unstable topological configurations of the surface. Second, by parameterizing the SDF as a cubic trivariate tensor-product B-spline function, we construct the implicitization with second-order smoothness and local control properties, enabling the rapid identification of all saddle points. Utilizing ray marching technique [Hart 1996], we developed an interactive system for topology and geometry editing that is user-friendly and intuitive to operate based on extensive user studies. We further demonstrate the effectiveness and usefulness of our system in a range of applications, including fixing surface reconstruction errors, artistic work design, 3D medical imaging and simulation, and virtual antiquity restoration.

Limitations. Our methodology, in its present form, has at least two limitations. First, it operates directly on the implicit representation, which can lead to slight deviations from the original surface due to the implicitization process. This issue is particularly pronounced for CAD models. Second, our current implementation relies on uniform

space partitioning, resulting in increased time and memory overhead for high-resolution scenarios.

Future works. We intend to define additional deformer templates to accommodate a wider variety of editing effects. Furthermore, we will add more buttons to the interactive system, such as copy, paste, undo, and redo, to improve the user experience. Additionally, we shall improve the implementation, specifically by exploring the potential of substituting the regular grid with an octree.

ACKNOWLEDGMENTS

The authors would like to thank the anonymous reviewers for their valuable comments and suggestions. This work is supported by National Key R&D Program of China (2022YFB3303200), National Natural Science Foundation of China (62002190, 62272277), and Natural Science Foundation of Shandong Province (ZR2020MF036).

REFERENCES

- Baptiste Angles, Marco Tarini, Brian Wyvill, Loïc Barthe, and Andrea Tagliasacchi. 2017. Sketch-based implicit blending. *ACM Transactions on Graphics (TOG)* 36, 6 (2017), 1–13.
- Andreas Bærentzen. 1998. Octree-based volume sculpting. In *IEEE Visualization*, Vol. 98. 9–12.
- Loïc Barthe, Benjamin Mora, Neil Dodgson, and Malcolm Sabin. 2002. Triquadratic reconstruction for interactive modelling of potential fields. In *Proceedings SML Shape Modeling International 2002*. IEEE, 145–275.
- Adrien Bernhardt, Loïc Barthe, Marie-Paule Cani, and Brian Wyvill. 2010. Implicit blending revisited. In *Computer Graphics Forum*, Vol. 29. Wiley Online Library, 367–375.
- Florian Canezin, Gaël Guennebaud, and Loïc Barthe. 2016. Topology-aware neighborhoods for point-based simulation and reconstruction. In *Eurographics/ACM SIGGRAPH Symposium on Computer Animation*.
- Paolo Cignoni, Marco Callieri, Massimiliano Corsini, Matteo Dellepiane, Fabio Ganovelli, and Guido Ranzuglia. 2008. MeshLab: an Open-Source Mesh Processing Tool. In *Eurographics Italian Chapter Conference*, Vittorio Scaramo, Rosario De Chiara, and Ugo Erra (Eds.). The Eurographics Association.
- Manolya Eyiyurekli and David Breen. 2010. Interactive free-form level-set surface-editing operators. *Computers & Graphics* 34, 5 (2010), 621–638.
- Eric Ferley, Marie-Paule Cani, and Jean-Dominique Gascuel. 2000. Practical volumetric sculpting. *The Visual Computer* 16, 8 (2000), 469–480.
- Eric Ferley, Marie-Paule Cani, and Jean-Dominique Gascuel. 2001. Resolution adaptive volume sculpting. *Graphical Models* 63, 6 (2001), 459–478.
- Barry Fowler. 1992. Geometric manipulation of tensor product surfaces. In *Proceedings of the 1992 symposium on Interactive 3D graphics*. 101–108.
- Hongbo Fu, Chiew-Lan Tai, and Hongxin Zhang. 2004. Topology-free cut-and-paste editing over meshes. In *Geometric Modeling and Processing, 2004. Proceedings. IEEE*, 173–182.
- Tinsley A Galyean and John F Hughes. 1991. Sculpting: An interactive volumetric modeling technique. *ACM SIGGRAPH Computer Graphics* 25, 4 (1991), 267–274.
- Olivier Gourmel, Loïc Barthe, Marie-Paule Cani, Brian Wyvill, Adrien Bernhardt, Mathias Paulin, and Herbert Grasberger. 2013. A gradient-based implicit blend. *ACM Transactions on Graphics (TOG)* 32, 2 (2013), 1–12.
- Charles A Hall and W Weston Meyer. 1976. Optimal error bounds for cubic spline interpolation. *Journal of Approximation Theory* 16, 2 (1976), 105–122.
- John C Hart. 1996. Sphere tracing: A geometric method for the antialiased ray tracing of implicit surfaces. *The Visual Computer* 12, 10 (1996), 527–545.
- John C Hart. 1998. Morse theory for implicit surface modeling. In *Mathematical Visualization*. Springer, 257–268.
- Magnus R Hestenes, Eduard Stiefel, et al. 1952. Methods of conjugate gradients for solving linear systems. *Journal of research of the National Bureau of Standards* 49, 6 (1952), 409–436.
- Ping Hu and Jian Wen. 2019. Research on 3D animation character design based on multimedia interaction. *Multimedia Tools and Applications* (2019), 1–14.
- Zhiyang Huang, Nathan Carr, and Tao Ju. 2019. Variational implicit point set surfaces. *ACM Transactions on Graphics (TOG)* 38, 4 (2019), 1–13.
- Tomohiko Ito, Teruyoshi Kaneko, Yoshiki Tanaka, and Sato Saga. 2021. Over-sketching operation to realize geometrical and topological editing across multiple objects in sketch-based CAD interface. In *26th International Conference on Intelligent User Interfaces-Companion*. 49–51.
- Alec Jacobson, Ladislav Kavan, and Olga Sorkine-Hornung. 2013. Robust inside-outside segmentation using generalized winding numbers. *ACM Transactions on Graphics (TOG)* 32, 4 (2013), 1–12.
- Alec Jacobson, Daniele Panozzo, et al. 2018. libigl: A simple C++ geometry processing library. <https://libigl.github.io/>.
- Tao Ju, Qian-Yi Zhou, and Shi-Min Hu. 2007. Editing the topology of 3D models by sketching. *ACM Transactions on Graphics (TOG)* 26, 3 (2007), 42–es.
- Michael Kazhdan and Hugues Hoppe. 2013. Screened poisson surface reconstruction. *ACM Transactions on Graphics (ToG)* 32, 3 (2013), 1–13.
- Sebastian Koch, Albert Matveev, Zhongshi Jiang, Francis Williams, Alexey Artemov, Evgeny Burnaev, Marc Alexa, Denis Zorin, and Daniele Panozzo. 2019. ABC: A Big CAD Model Dataset For Geometric Deep Learning. In *The IEEE Conference on Computer Vision and Pattern Recognition (CVPR)*.
- Kai lin Yu and Yung-Chin Tsao. 2022. A STUDY OF CHARACTER DESIGN METHOD. *International Journal of Organizational Innovation* 15, 1 (2022).
- Avirup Mandal, Parag Chaudhuri, and Subhasis Chaudhuri. 2022. Interactive physics-based virtual sculpting with haptic feedback. *Proceedings of the ACM on Computer Graphics and Interactive Techniques* 5, 1 (2022), 1–20.
- Joss Kingdom Moo-Young, Andrew Hogue, and Veronika Szukdlarek. 2021. Virtual materiality: Realistic clay sculpting in vr. In *Extended Abstracts of the 2021 Annual Symposium on Computer-Human Interaction in Play*. 105–110.
- Bernard Mourrain and Jean Pascal Pavone. 2009. Subdivision methods for solving polynomial equations. *Journal of Symbolic Computation* 44, 3 (2009), 292–306.
- Ken Museth, David E Breen, Ross T Whitaker, and Alan H Barr. 2002. Level set surface editing operators. In *Proceedings of the 29th annual conference on Computer graphics and interactive techniques*. 330–338.
- Ken Museth, David E Breen, Ross T Whitaker, Sean Mauch, and David Johnson. 2005. Algorithms for interactive editing of level set models. In *Computer Graphics Forum*, Vol. 24. Wiley Online Library, 821–841.
- Galina I Pasko, Alexander A Pasko, and Tosiya L Kunii. 2005. Bounded blending for function-based shape modeling. *IEEE Computer Graphics and Applications* 25, 2 (2005), 36–45.
- Mengqi Peng, Jun Xing, and Li-Yi Wei. 2018. Autocomplete 3d sculpting. *ACM Transactions on Graphics (TOG)* 37, 4 (2018), 1–15.
- Ronald N Perry and Sarah F Frisken. 2001. Kizamu: A system for sculpting digital characters. In *Proceedings of the 28th annual conference on Computer graphics and interactive techniques*. 47–56.
- Mohammad Rouhani, Angel D Sappa, and Edmond Boyer. 2014. Implicit B-spline surface reconstruction. *IEEE Transactions on Image Processing* 24, 1 (2014), 22–32.
- Ryan Schmidt, Brian Wyvill, and Eric Galin. 2005. Interactive implicit modeling with hierarchical spatial caching. In *International Conference on Shape Modeling and Applications 2005 (SMI'05)*. IEEE, 104–113.
- Andrei Sharf, Thomas Lewiner, Gil Shklarski, Sivan Toledo, and Daniel Cohen-Or. 2007. Interactive topology-aware surface reconstruction. *ACM Transactions on Graphics (TOG)* 26, 3 (2007), 43–es.
- Barton T. Stander and John C. Hart. 1997. Guaranteeing the Topology of an Implicit Surface Polygonization for Interactive Modeling. In *Proceedings of the 24th Annual Conference on Computer Graphics and Interactive Techniques (SIGGRAPH '97)*. ACM Press/Addison-Wesley Publishing Co., USA, 279–286. <https://doi.org/10.1145/258734.258868>
- Yizhi Tang and Jieqing Feng. 2018. Multi-scale surface reconstruction based on a curvature-adaptive signed distance field. *Computers & Graphics* 70 (2018), 28–38.
- Demetri Terzopoulos and Hong Qin. 1994. Dynamic NURBS with geometric constraints for interactive sculpting. *ACM Transactions on Graphics (TOG)* 13, 2 (1994), 103–136.
- Janis PY Wong, Rynson WH Lau, and Lizhuang Ma. 2000. Virtual 3d sculpting. *The Journal of Visualization and Computer Animation* 11, 3 (2000), 155–166.
- Huang Xiong and Yao Zimin. 2022. Algorithm modeling technology of computer aided fractal art pattern design. In *2022 World Automation Congress (WAC)*. IEEE, 62–65.
- Kangxue Yin, Hui Huang, Hao Zhang, Minglun Gong, Daniel Cohen-Or, and Baoquan Chen. 2014. Morfit: interactive surface reconstruction from incomplete point clouds with curve-driven topology and geometry control. *ACM Trans. Graph.* 33, 6 (2014), 202–1.
- Qingnan Zhou and Alec Jacobson. 2016. Thingi10K: A Dataset of 10,000 3D-Printing Models. *arXiv preprint arXiv:1605.04797* (2016).

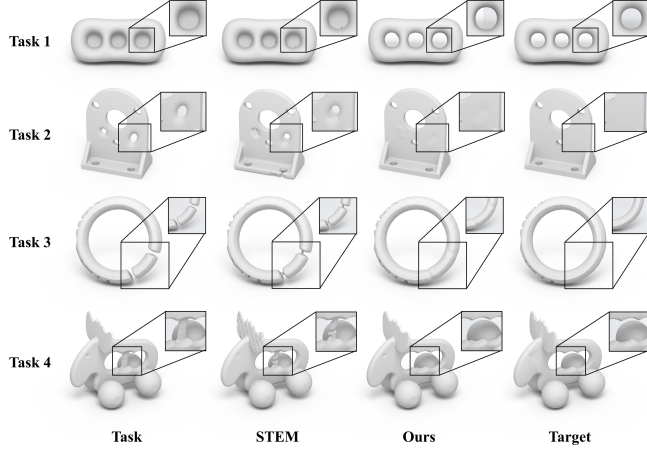


Fig. 9. Test our system and STEM [Ju et al. 2007] by conducting four target reproduction tasks. It can be seen from the highlighted differences that our system is capable of more effectively restoring real topological and geometric structures.

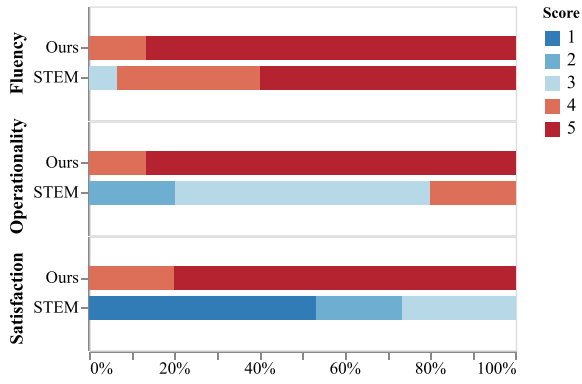


Fig. 10. Statistics about fluency, operability and satisfaction based on the questionnaire.

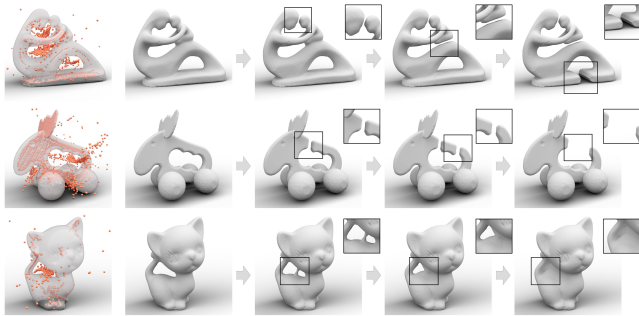


Fig. 11. Examples of the creative process exclusively achieved through topology editing. The entire process comprises two parts: saddle point localization (orange balls in leftmost column) and interactive editing (right four columns).

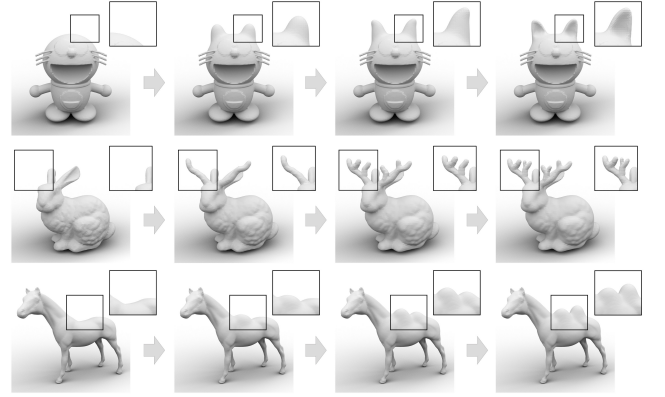


Fig. 12. Examples of the creative process exclusively achieved through geometry editing.

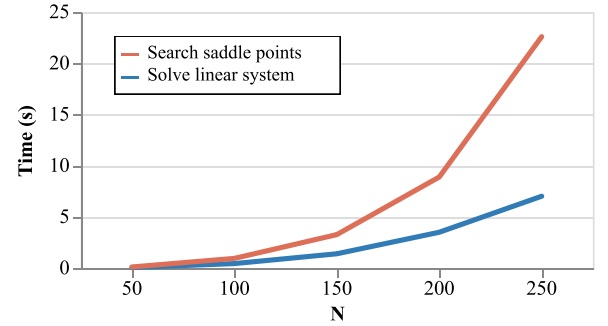


Fig. 13. Timing costs with regard to the grid resolution along an axis.

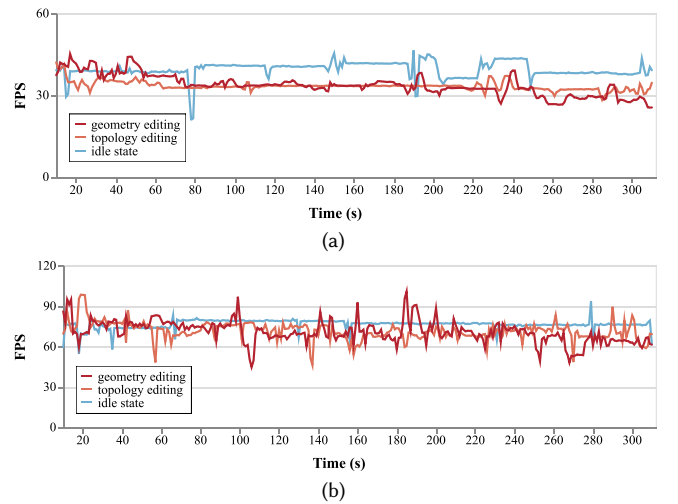


Fig. 14. FPS statistical results for topology editing, geometry editing, and idle state on NVIDIA GeForce GTX 1060 (a) and NVIDIA GeForce RTX 3060 (b) GPUs.

Table 2. Quantitative comparison for topology editing. We present the average values to assess the results produced by volunteers.

	Chamfer ↓		F-Score ↑		Normal C. ↑		Genus			Components		
	Ours	STEM [2007]	Ours	STEM [2007]	Ours	STEM [2007]	Ours	STEM [2007]	GT	Ours	STEM [2007]	GT
Task 1	2.80	3.84	94.00	91.46	98.68	94.50	3.14	3.20	3	1.00	1.43	1
Task 2	2.86	3.72	93.62	84.21	98.02	94.14	8.15	7.67	8	1.08	1.77	1
Task 3	2.96	4.33	92.78	84.41	96.69	92.26	1.00	5.54	1	1.00	1.13	1
Task 4	2.65	4.14	94.36	79.40	99.22	94.58	1.00	3.92	1	1.00	1.00	1

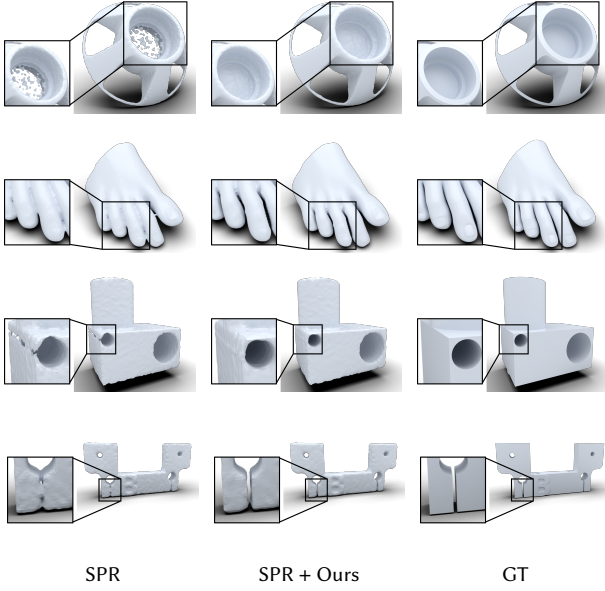


Fig. 15. We sampled 10K points from the ground-truth models (right) using random sampling, and reconstructed the surface using Screened Poisson Reconstruction (SPR) [Kazhdan and Hoppe 2013] with ground truth normals. The reconstruction results (left) deviate from the ground truth shape and contain various structural artifacts due to point insufficiency. However, with our interactive system, these structural artifacts can be easily addressed (middle). It is worth noting that the four models are from the ABC [Koch et al. 2019] dataset and Thing10K [Zhou and Jacobson 2016] dataset.

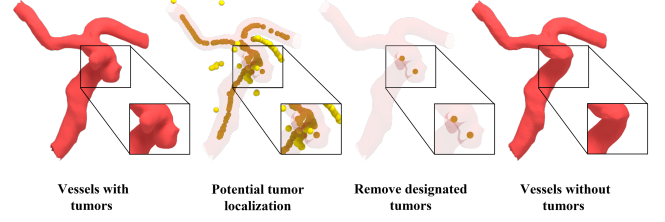


Fig. 17. With the use of our interactive system, doctors are able to quickly locate vascular tumors and remove them from the original model, resulting in a virtually healed vessel model.

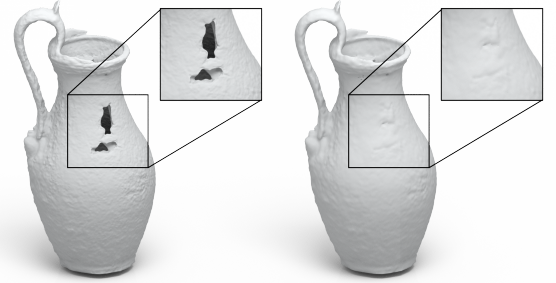


Fig. 18. The restoration outcome of an ancient Roman wine-jug by utilizing our interactive system.



Fig. 16. Taking the short honey pot (left) as the base model, we allow users to edit the topology according to their own wishes, yielding two creative artistic designs (middle, right).